ACS OMEGA

http://pubs.acs.org/journal/acsodf

Article

Improvement of the Gas Barrier Properties of PLA/OMMT Films by Regulating the Interlayer Spacing of OMMT and the Crystallinity of PLA

Fenfen Li, Caili Zhang,* and Yunxuan Weng*

Cite This: *ACS Omega* 2020, 5, 18675−18684

Read Online

ACCESS | Metrics & More | Article Recommendations | Supporting Information

ABSTRACT: A high gas barrier performance should be ensured in case of biodegradable packing applications. However, the gas barrier properties of the biodegradable poly(lactic acid) (PLA) are not much effective. Nanocomposites can provide innovative solutions to enhance the barrier performance. In this study, different weight percentages of organically modified montmorillonite (OMMT) (0, 2, 4, 6, 8, and 10 wt %)-incorporated PLA/OMMT nanocomposites were prepared by melt mixing. Ethylene glycol diglycidyl ether (EGDE) was used to regulate the interlayer spacing of OMMT and increase the PLA crystallinity to further improve the gas barrier performance of the PLA/OMMT films. The crystallinity of PLA was significantly improved because EGDE-modified OMMT served as an efficient nucleating agent. The PLA/EGDE/OMMT films demonstrated a unique structure such that the adjacent OMMT layers were linked through the PLA crystals that serve as a bridge with respect to the spaces between the OMMT layers. The O_2 permeability of the PLA/EGDE4/OMMT-6 film decreased by approximately 79% when compared with that of the neat PLA film. X-ray diffraction and differential scanning calorimetry analyses denoted that the reduced oxygen permeability of the PLA/EGDE4/OMMT-6 film can be primarily attributed to the high crystallinity of the PLA matrix and the bridging effect of the PLA crystals between two adjacent layers. Based on the experimental results, the relation between the relative permeability and vol % OMMT is in good agreement with that of the predicted values obtained using the Bharadwaj model when $S = 0$. The added EGDE weakened the thermal stability and tensile strength, mainly because of degradation of the hydroxyl groups of EGDE formed by epoxy ring opening, and these hydroxyl groups can promote PLA matrix degradation. However, the practical application temperature of the packaging film is considerably lower than the thermal decomposition temperature; therefore, the reduction of the thermal decomposition temperature does not affect the use of the packaging film.

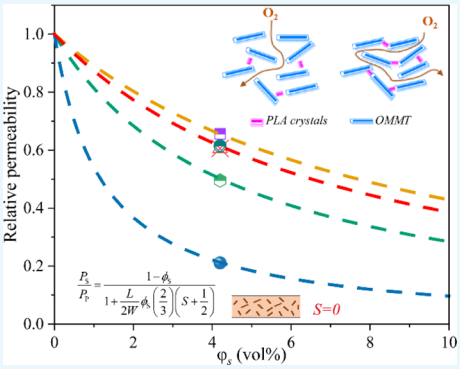

1. INTRODUCTION

The usage of novel and efficient polymer materials based on nanocomposites for food packaging can provide innovative solutions to enhance the polymer performance. They also exhibit certain economic and environmental advantages when compared with the pristine polymers, including an increase in biodegradability, improved barrier properties with respect to gases and light, an increase in thermal stability, improved mechanical properties, and a reduction in the volume of waste material for landfill disposal.[1−4]

Poly(lactic acid) (PLA) is an important biodegradable polymer obtained based on lactic acid produced via the fermentation of polysaccharides such as corn or potato starch. PLA can entirely degrade into carbon dioxide and water under specific natural conditions.[5] It exhibits broad application potential with respect to packaging materials because of its high degradability and transparency, good mechanical strength, and processability.[6,7] However, the barrier properties of neat PLA are less effective when compared with those of the traditional materials (e.g., metal and glass), limiting its wide application as a packaging material.[8] Thus, the polymeric nanocomposites obtained by incorporating impermeable fillers (nanoplatelets) into a polymer matrix have been utilized to fabricate high-barrier-performance polymer films.[7,9−11]

Montmorillonite (MMT) is a natural clay having a high specific surface area that can potentially produce the "nanobarrier walls" within the nanocomposites. Thus, the diffusing gas molecules must travel along long and tortuous pathways through nanocomposites because of the unique laminar structure of MMT.[10] We must develop a homogeneous dispersion of MMT throughout the polymer matrix to ensure that the addition of MMT can be advantageously utilized. The morphological arrangement of MMT within the

Received: March 28, 2020
Accepted: July 9, 2020
Published: July 21, 2020

Scheme 1. (a) Molecular Structure of OMMT Containing $HOOC(CH_2)_{17}NH_3^+$ and (b) Schematic of the Side View between the Layers

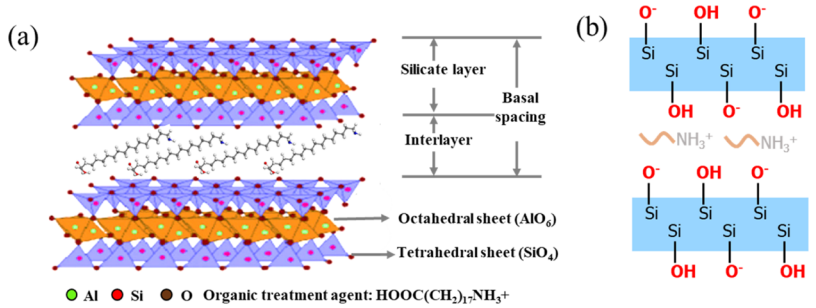

polymer matrix is determined based on the entropic and enthalpic factors.[12,13] However, organically modified montmorillonite (OMMT) is used to achieve an improved dispersion effect within the matrix because the hydrophilic clay exhibits poor compatibility with the polymer matrix.[14−20] The gas barrier properties should improve in the presence of OMMT.

Koh et al. decreased the O_2 permeability of PLA by 31% by adding 0.8 wt % OMMT (Closite 15A),[17] and Sabet and Katbab decreased the O_2 permeability of PLA by 26% by adding 3 wt % OMMT (MMT modified with methyl tallow bis(2-hydroxyethyl) ammonium).[18] Further, Ray et al. decreased the O_2 permeability of PLA by 19% by adding 7 wt % OMMT (MMT modified with a trimethyl octadecylammonium cation),[19] and Picard et al. added 8 wt % OMMT (MMT modified with a dihydroxymethyl tallow quaternary ammonium cation) to decrease the O_2 permeability of PLA by 24%.[20] These results demonstrate that when the concentration of OMMT reaches a certain level, its content does not considerably affect the barrier performance of the films. This is mainly because the morphology of OMMT in the polymer matrix significantly influences the gas barrier properties. In a previously conducted study related to polymer nanocomposites in case of the gas barrier applications, it was observed that less than 10 vol % of the filler contents is sufficient when adding layered nanoparticles.[21] With respect to OMMT in nanocomposites, the volume fraction, morphology (i.e., exfoliation, dispersion, and orientation), and aspect ratio are the three main factors affecting the barrier performance of the nanocomposite films in case of the diffusion of gas molecules.[22,23] However, the gas barrier performance of the nanocomposite films containing a high volume of OMMT will remain low. Because excessive OMMT will agglomerate in the PLA matrix, the diffusing path of O_2 molecules will be shorter.

In this research, we develop a new process that combines the impermeability of OMMT and the physical barriers of PLA crystals to further improve the gas barrier performance of PLA/OMMT films. The molecular structure of OMMT and the side view between the layers are presented in Scheme 1a,b. Ethylene glycol diglycidyl ether (EGDE) is used to regulate the interlayer spacing of OMMT and increase the PLA crystallinity.

2. EXPERIMENTAL SECTION

2.1. Materials. Commercially available PLA (4032D, M_n = 1.06 × 10^5 g/mol, M_w = 2.23 × 10^5 g/mol) was supplied by Nature Works using approximately 2% D-lactic acid (D-LA). OMMT (I.24TL) with a length/thickness of 80 was purchased from Nanocor Inc. (USA), and the organic treatment agent used in this product was 18-amino stearic acid ($HOOC(CH_2)_{17}NH_3^+$). OMMT and PLA were dried in an oven at 80 °C for 12 h before processing. Finally, EGDE (M_n = 174.19 g/mol) was obtained from Shanghai Macklin Biochemical Technology Co., Ltd. (China).

2.2. PLA/OMMT Composite Film Preparation. An internal mixer (Haake Rheometer) was used to fabricate PLA/OMMT nanocomposites with or without the EGDE agent. The internal mixer was operated at 180 °C and a rotation speed of 60 rpm for 5 min. Subsequently, the nanocomposite plates disintegrated into granules. Further, they were compression-molded into 60−90 μm thick films using a hydraulic press at 180 °C and 10 MPa. OMMT, PLA, and a compatibilizer were added into the internal mixer at a specific ratio. When preparing the PLA/OMMT nanocomposite film, the OMMT contents were varied between 2, 4, 6, 8, and 10 wt %, and the samples were designated as PLA/OMMT-2, PLA/OMMT-4, PLA/OMMT-6, PLA/OMMT-8, and PLA/OMMT-10, respectively. When preparing the PLA/EGDE/OMMT nanocomposite films, the OMMT content was determined as 6 wt % (PLA/OMMT-6), and PLA/OMMT nanocomposite materials containing varying EGDE contents of 1, 2, 4, and 6 phr were prepared in the same manner as mentioned above, with the samples being designated as PLA/EGDE1/OMMT-6, PLA/EGDE2/OMMT-6, PLA/EGDE4/OMMT-6, and PLA/EGDE6/OMMT-6, respectively. All the dried samples were stored in self-sealing bags to prevent any influence of moisture before performing characterization. The details of the sample formulas are presented in Table 1.

2.3. Characterization. The samples were subjected to X-ray diffraction (XRD) using an X-ray diffractometer (Bruker D8 ADVANCE, Bruker Daltonics Inc., Germany), whose Cu radiation source operates at 40 kV and 40 mA. The step size

Table 1. Preparation Formula of the PLA/OMMT Nanocomposite Films with and without EGDE

sample codes	PLA (wt %)	OMMT (wt %)	EGDE (phr)
neat PLA	100	0	
PLA/OMMT-2	98	2	
PLA/OMMT-4	96	4	
PLA/OMMT-6	94	6	
PLA/OMMT-8	92	8	
PLA/OMMT-10	90	10	
PLA/EGDE1/OMMT-6	94	6	1
PLA/EGDE2/OMMT-6	94	6	2
PLA/EGDE4/OMMT-6	94	6	4
PLA/EGDE6/OMMT-6	94	6	6

https://dx.doi.org/10.1021/acsomega.0c01405
ACS Omega 2020, 5, 18675−18684

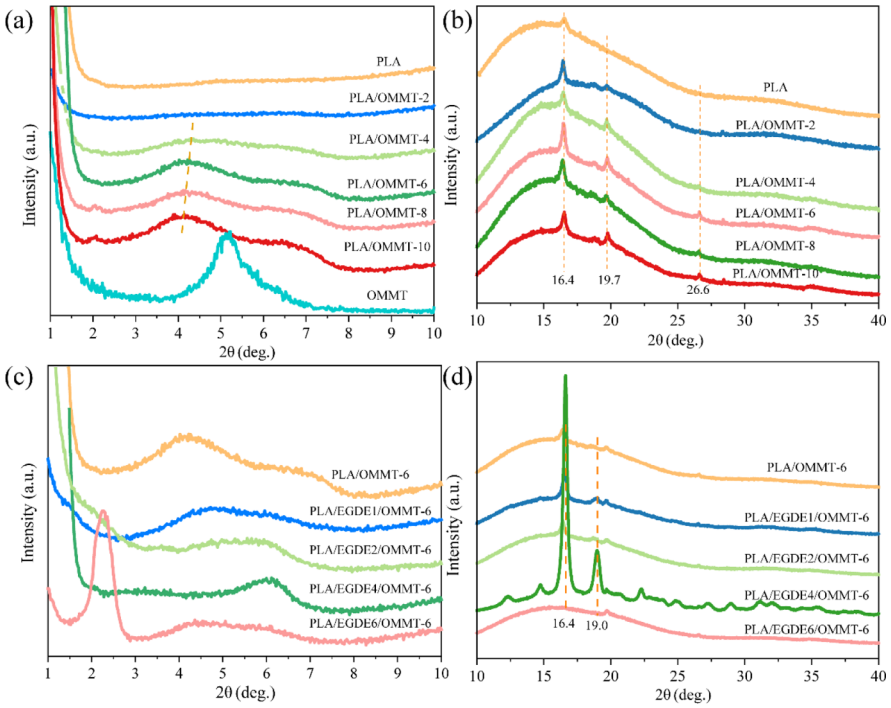

Figure 1. XRD patterns of (a,b) PLA/OMMT nanocomposites with varying OMMT contents and (c,d) PLA/OMMT-6 nanocomposites with varying EGDE contents.

Table 2. XRD Parameters of OMMT, PLA, and PLA/OMMT Nanocomposites

samples	2θ (1−10°)	d-spacing nm	2θ (10−40°)	d-spacing nm
OMMT	5.22	1.69		
PLA			16.4	0.54
PLA/OMMT-2			16.4, 19.7	0.54, 0.45
PLA/OMMT-4	4.28	2.05	16.4, 19.7	0.54, 0.45
PLA/OMMT-6	4.22	2.09	16.4, 19.7, 26.6	0.54, 0.45, 0.33
PLA/OMMT-8	4.16, 6.80	2.11, 1.30	16.4, 19.7, 26.6	0.54, 0.45, 0.33
PLA/OMMT-10	4.14, 6.80	2.12, 1.30	16.4, 19.7, 26.6	0.54, 0.45, 0.33
PLA/EGDE1/OMMT-6	4.72	1.86	16.4, 19.0	0.54, 0.46
PLA/EGDE2/OMMT-6	5.94	1.48	16.4, 19.0	0.54, 0.46
PLA/EGDE4/OMMT-6	6.12	1.44	16.4, 19.0	0.54, 0.46
PLA/EGDE6/OMMT-6	2.28, 4.36	3.86, 2.02	19.7	0.45

was 0.02°, and the scan speed was 2°/min at 0.6−40°. Further, we investigated the dispersion of OMMT in the polymer matrix based on the interlayer distance obtained by considering the disruption of the crystal structure. Bragg's law was used to calculate the interlayer distance of OMMT.

Scanning electron microscopy (SEM) analysis of the freezing fractured PLA/OMMT nanocomposite specimens was conducted using a Phenom Pro machine (Phenom World, Netherlands) at an acceleration voltage of 10 kV.

The differential scanning calorimetry (DSC) measurements were performed using a Q20 differential scanning calorimeter (TA Instruments, USA). The samples were stored in sealed aluminum pans and initially heated from 30 to 190 °C at a heating rate of 10 °C/min, which was followed by cooling from 190 to 30 °C at a rate of 20 °C/min. The second cycle involved heating from 30 to 190 °C at a heating rate of 10 °C/min. The fusion heat was determined based on the area under the melting peaks, which can be calculated by integrating the melting enthalpy. The degree of crystallinity (χ_c) of pure PLA and the composites can be calculated using eq 1

$$\chi_c = \frac{\Delta H_m - \Delta H_{cc}}{w\Delta H_m^0} \times 100\% \quad (1)$$

where ΔH_m denotes the experimental melting enthalpy (J/g), ΔH_m^0 is the melting enthalpy of 100% crystalline PLA (93.7 J/g), and w is the weight fraction of PLA in the composites.[24]

Gas permeation analysis of the PLA/OMMT nanocomposite films with a film area of 10 cm^2 was conducted using an oxygen transmission rate tester 31M (Labthink, China) at 23 °C with a relative humidity of 30% according to the ASTM D3985 standard.[25]

The thermal stability data of the PLA/OMMT composites were obtained by mounting 5−10 mg of the samples onto platinum pans, and these composites were placed in a thermogravimetric analyzer (STA-7200, HITACHI, Japan). The loss of temperature and weight was recorded at 30−500 °C at a heating rate of 10 °C/min when the N_2 gas purging flow was 40 mL/min.

The tensile properties of the samples were verified using an electric tensile tester (Shenzhen Labsans Material Testing Co., Ltd., China) at a speed of 5 mm/min, with reference to the

https://dx.doi.org/10.1021/acsomega.0c01405
ACS Omega 2020, 5, 18675−18684

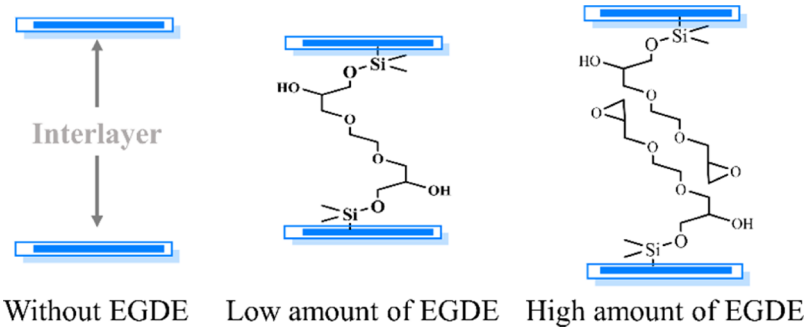

Figure 2. Interlayer spacing of OMMT without adding EGDE and after cross-linking using different amounts of EGDE.

ASTM D882 standard. Finally, we reported the average values for at least five specimens for all the tests.

3. RESULTS AND DISCUSSION

3.1. XRD Study. We performed XRD measurements for evaluating the interlayer changes of OMMT and the crystalline structures of the PLA-based nanocomposites. Figure 1 illustrates the XRD curves of OMMT, neat PLA, and PLA/OMMT nanocomposites with different amounts of EGDE within 1−40°. The 2θ values obtained based on these curves and the interlayer spacing values calculated based on Bragg's law are presented in Table 2. The 2θ values of pure OMMT and OMMT in the nanocomposites largely correspond with 1−10°, whereas the 2θ values of neat PLA and PLA in the nanocomposites largely correspond with 10−40°. Figure 1a shows that the primary (001) diffraction peak of OMMT can be observed at 2θ = 5.22°, corresponding to an interlayer spacing of 1.69 nm, whereas PLA did not have any peaks in 1−10°. In the case of PLA/OMMT-2 and PLA/OMMT-4, a very subtle characteristic peak can be observed in the XRD curves, indicating that OMMT was fully exfoliated. By increasing the OMMT concentration, the (001) characteristic peak of the nanocomposites strengthened and the interlayer spacing only slightly changed. However, with a further increase in OMMT content (greater than 6%), a number of layer stacks produced a new peak at 2θ = 6.8°. This is mainly because the layers are difficult to disperse, resulting in a certain amount of aggregation.[19]

Figure 1b shows that the main characteristic diffraction peak of neat PLA was at 2θ = 16.4°, corresponding to the (110)/(200) diffraction peak.[26,27] At the same time, for the PLA/OMMT nanocomposites, a new peak can be observed at 2θ = 19.7°, corresponding to the (203)/(113) characteristic diffraction peak. With the addition of OMMT into PLA, the intensity of the (110)/(200) and (203)/(113) diffraction peaks initially increased before decreasing with an increase in OMMT loading, indicating that the crystallinity of the nanocomposite with a 6 wt % loading of OMMT was higher than that of the remaining PLA/OMMT nanocomposites. Therefore, at a low loading level, intercalated and exfoliated OMMT served as a nucleating agent, indicating that the crystallinity of the nanocomposite improved.[28] At the same time, because of layer aggregation with increasing OMMT content (greater than 6%), the PLA chain arrangement was hindered and the crystallinity of the PLA/OMMT nanocomposites decreased.[29] Therefore, PLA/OMMT-6 was selected as the optimal sample for the subsequent cross-linking procedure.

Figure 1c shows that with increasing amount of EGDE, the 2θ values of the (001) diffraction peak initially increased and subsequently decreased, indicating that the interlayer spacing of OMMT displayed an opposite behavior, that is, the interlayer spacing initially decreased and subsequently increased. This is mainly because two hydroxyl groups reacted with one molecule of EGDE at low EGDE concentrations, and the distance between two interlayers decreased with an increase in EGDE loading (increasing number of hydroxyl groups cross-linked with the epoxy groups of EGDE). PLA/EGDE4/OMMT-6 exhibited the lowest interlayer spacing, with a value of 1.44 nm. However, one hydroxyl group will react with one molecule of EGDE, and the distance between the two interlayers will drastically increase when the concentration of EGDE is sufficiently high. Meanwhile, PLA/EGDE6/OMMT-6 demonstrated the highest interlayer spacing, with a value of 3.86 nm.

Figure 1d shows that the sample with the lowest interlayer spacing, PLA/EGDE4/OMMT-6, exhibited the highest intensity of diffraction peaks, indicating that the highest crystallinity of the PLA matrix could be observed in nanocomposites containing 4 phr EGDE. As noted above, OMMT serves as a nucleating agent to promote the crystallization of PLA. After the addition of EGDE, the crystallinity of PLA in the nanocomposites significantly improved because the linear chains of EGDE served as nucleating agents to enhance crystallization.

In conclusion, as illustrated in Figure 2, on one hand, the hydroxyl groups on the OMMT surface could react with the EGDE epoxy groups, and the amount of EGDE could regulate the interlayer spacing of OMMT. The cross-link reaction between OMMT and EGDE was confirmed by attenuated total reflection (ATR) spectra, as shown in Figure S1. A new peak at 691 cm^{-1} occurred in PLA/EGDE/OMMT-6, which corresponds to the Si−O−C bond. This can prove that the cross-link reaction occurred between the Si−OH group of OMMT and the epoxy group of EGDE. On the other hand, the crystallinity of the PLA matrix within the nanocomposites is significantly improved because EGDE could act as a nucleating agent to enhance the crystallization. The crystallinity of the PLA/OMMT composites with and without EGDE cross-linking agents will be revealed based on the DSC measurement.

3.2. Crystallization and Melting Behaviors. The EGDE cross-linking agents in the PLA/OMMT nanocomposites can decrease the interlayer spacing, indicating that the adjacent layers of OMMT will be connected by the crystal between two layers. Because of this connection effect, in terms of OMMT with the addition of EGDE, the aspect ratio significantly

https://dx.doi.org/10.1021/acsomega.0c01405
ACS Omega 2020, 5, 18675−18684

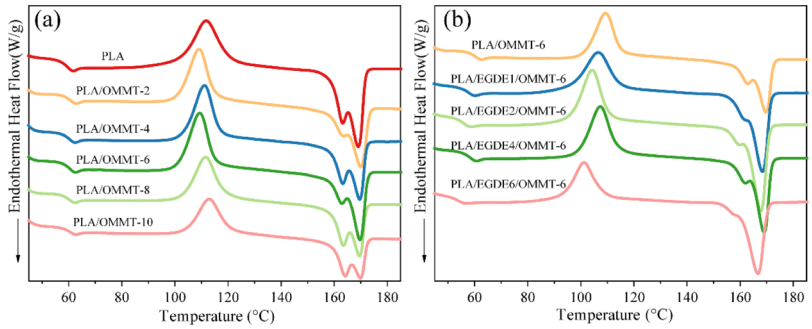

Figure 3. DSC curves of (a) PLA/OMMT nanocomposites with different OMMT contents and (b) PLA/OMMT-6 nanocomposites with different EGDE contents.

Table 3. DSC Data and Crystallinity Obtained by Wide-Angle X-Ray Diffraction (WAXD) Characterization for PLA/OMMT Composites with Different OMMT and EGDE Contents

samples	T_g (°C)	T_{cc} (°C)	T_{m1} (°C)	T_{m2} (°C)	ΔH_{cc} (J/g)	ΔH_m (J/g)	$\chi_{c\text{-DSC}}$ (%)	$\chi_{c\text{-WAXD}}$ (%)
neat PLA	58.9	112.8	163.1	170.8	23.67	24.81	1.23	0.73
PLA/OMMT-2	58.4	108.8	163.5	169.8	23.70	25.76	2.26	1.85
PLA/OMMT-4	59.1	110.0	163.2	169.6	24.12	26.87	3.08	2.72
PLA/OMMT-6	58.7	109.2	162.8	169.7	24.52	27.24	3.11	2.93
PLA/OMMT-8	58.8	111.4	163.4	169.7	24.15	26.55	2.80	2.82
PLA/OMMT-10	59.2	112.7	164.2	170.0	23.24	25.84	3.10	2.90
PLA/EGDE1/OMMT-6	56.2	106.4		168.4	24.53	28.76	4.83	3.95
PLA/EGDE2/OMMT-6	55.0	104.1		167.7	24.25	32.52	9.45	11.87
PLA/EGDE4/OMMT-6	56.5	107.1		169.0	25.84	34.83	10.28	22.75
PLA/EGDE6/OMMT-6	56.2	104.0		167.9	23.96	30.92	7.95	0.71

Table 4. Summary of the Results with Respect to the Oxygen Transmission Rate of the PLA/OMMT Composites with Different OMMT Loadings

	OMMT content		O_2 permeability			
Sample	(wt %)	(vol %)	barrer[a]	10^{-14} cm^3 cm/cm^2 s Pa	reduction (%)	test condition
neat PLA	0	0	0.218 ± 0.015	1.635 ± 0.11	0	23 °C with a relative humidity of 30% according to the ASTM D3985 standard
PLA/OMMT-2	2	1.4	0.154 ± 0.01	1.155 ± 0.08	29.4	
PLA/OMMT-4	4	2.8	0.141 ± 0.007	1.058 ± 0.05	35.3	
PLA/OMMT-6	6	4.2	0.132 ± 0.01	0.990 ± 0.08	39.4	
PLA/OMMT-8	8	5.6	0.151 ± 0.02	1.133 ± 0.15	30.7	
PLA/OMMT-10	10	7.0	0.158 ± 0.03	1.185 ± 0.23	27.5	
PLA/EGDE1/OMMT-6	6	4.2	0.134 ± 0.012	1.005 ± 0.09	38.5	
PLA/EGDE2/OMMT-6	6	4.2	0.108 ± 0.01	0.810 ± 0.08	50.5	
PLA/EGDE4/OMMT-6	6	4.2	0.046 ± 0.005	0.345 ± 0.38	78.9	
PLA/EGDE6/OMMT-6	6	4.2	0.143 ± 0.01	1.073 ± 0.08	34.4	
PLA/1.37 vol % GONS[30]				1.145	45	RT, 50% RH
PLA/0.4 wt % GO[31]				1.2	68	25 °C
PLA/0.8 wt % OMMT[17]	0.8		0.34		29	30 °C
PLA/3 wt % OMMT[18]	3				26	ASTM 1434-82
PLA/7 wt % OMMT[19]	7				19	20 °C and 90% RH
PLA/8 wt % OMMT[20]	8		0.38		24	20 °C

[a]1 barrer = 1 × 10^{-10} cm^3 (STP) cm/cm^2 s cm Hg = 7.5 × 10^{-18} m^2/s Pa = 7.5 × 10^{-14} cm^3 (STP) cm/cm^2 s Pa; 1 Pa = 7.5005 × 10^{-4} cm Hg.

increased with the increasing crystallinity of PLA between adjacent lamellae. To examine this phenomenon, the DSC heating curves of neat PLA and the OMMT nanocomposite films with and without the EGDE cross-linking agents were determined, as shown in Figure 3. The glass-transition temperature (T_g), cold crystallization temperature (T_{cc}), melting temperature (T_m), and crystallinity (χ_c) data are presented in Table 3.

As depicted in Figure 3a, with increasing OMMT content, T_{cc} reduced and the crystallinity of the PLA matrix was slightly modified. With the incorporation of 6 wt % OMMT into PLA, the crystallinity increased from 1.23 to 3.11%. Once the mass fraction of OMMT became more than 6 wt %, T_{cc} shifted to a high-temperature region, whereas the crystallinity did not increase any further. These results imply that an appropriate amount of OMMT provides heterogeneous nucleating sites to enhance the cold crystallization ability of PLA, whereas the

https://dx.doi.org/10.1021/acsomega.0c01405
ACS Omega 2020, 5, 18675−18684

movement of the PLA chain is restricted by an OMMT overload.

After the addition of EGDE into the composites, as shown in Figure 3b, the T_g and T_{cc} of PLA decreased, and the crystallinity of PLA improved compared with that of PLA/OMMT without adding EGDE. With an increase in the amount of EGDE, the χ_c of PLA initially increased and subsequently decreased, which is in accordance with the aforementioned XRD study and the oxygen permeation performance. The crystallinity increased from 3.11 to 10.28% with the addition of 4 phr EGDE into PLA/OMMT-6. When the addition of EGDE was 4 phr, most of EGDE could react with OMMT. EGDE-modified OMMT could act as a nucleating agent to increase the crystallinity of PLA. The high crystallinity of PLA can be explained in terms of the strong heterogeneous nucleation effect in the presence of EGDE-modified OMMT. However, when the addition of EGDE was greater than 4 phr, there was some unreacted EGDE in the composite, which can act as a plasticizer. EGDE was inserted between the PLA chains, making the interaction force between the PLA chains weaker and the rearrangement ability weaker. Therefore, the crystallinity of PLA was remarkably decreased. Thus, our stated assumption, that is, the newly formed crystalline region between two adjacent layers could serve as a bridge for connecting several OMMT layers into a whole, can be confirmed. The closer the distance between the lamellae, the higher the crystallinity and the greater the probability of connection.

Therefore, the remarkable enhancement of the barrier properties of the PLA/EGDE4/OMMT-6 film can be mainly attributed to the crystals between adjacent layers, their impermeable properties, and bridging effects because of the high oxygen barrier performance.

3.3. Gas Barrier Properties. The oxygen permeability (P_{O_2}) of the PLA/OMMT nanocomposite films with or without EGDE cross-linking agents was used to characterize the barrier properties of the films, and the results are presented in Table 4. Figure 4 shows the plot of the oxygen permeability

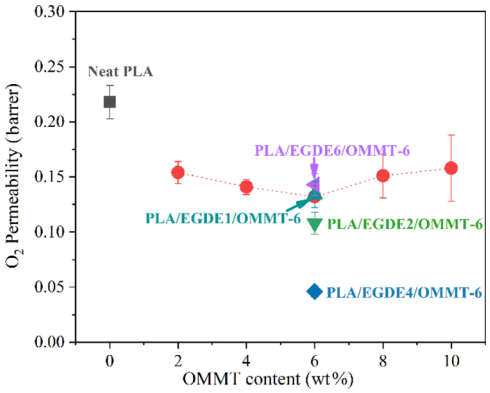

Figure 4. O_2 permeability of the PLA/OMMT nanocomposites with various OMMT contents and EGDE cross-linking agents.

as a function of the OMMT mass fraction based on the data obtained from Table 4 for the films with or without EGDE; this allows for a considerably intuitive comparison of the gas barrier performance. Specifically, an approximate reduction of 39.4% could be observed with respect to P_{O_2} from 0.218 to 0.132 barrer by adding 6 wt % OMMT (PLA/OMMT-6). However, P_{O_2} increased when the OMMT content was higher than 6 wt %. This behavior can be attributed to the poor dispersion of OMMT in the PLA matrix, resulting in several defects with respect to the film structure.

The oxygen permeability of the PLA/OMMT-6 film decreased with the addition of EGDE. The P_{O_2} of the nanocomposite films initially decreased and subsequently increased with an increase in the EGDE content, and the addition of 4 phr EGDE into the composites resulted in the highest oxygen barrier performance. Specifically, PLA/EGDE4/OMMT-6 demonstrated a reduction of approximately 79% (0.218−0.046 barrer) with respect to P_{O_2} when compared with the neat PLA film. As presented in Table 3, the PLA/EGDE4/OMMT-6 film exhibited a considerably better barrier performance when compared with those exhibited by the remaining PLA-based nanocomposites with OMMT or graphene oxide (GO) nanosheets.

Compared with the commercial plastic packaging films, the PLA/EGDE4/OMMT-6 film exhibited a considerably better barrier performance when compared with those exhibited by poly(vinyl acetate), polyethylene (PE), polystyrene, and cellulose acetate.[32−35] This barrier performance is comparable to the gas barrier performance of the poly(vinyl chloride) and poly(ethylene terephthalate) films even though it is inferior to the performance of the poly(viny1 alcohol) and poly(vinylidene fluoride) films, which are two types of commercial films exhibiting the highest barrier performance.[36−39]

The reduction in the gas permeability of the films could be related to (1) the tortuosity effect induced by incorporating an impermeable nanoplate, (2) the modification of the properties of the polymer matrix (e.g., free volume of the polymer, crystallinity, and nucleating effect of the particles), and (3) the modification of the sorption sites for the sorption of the penetrating molecule.[21,40] In this study, the gas barrier performance of the PLA/OMMT-6 films was varied after the addition of different amounts of EGDE. This can be majorly attributed to the increase in the crystallinity of the polymer matrix and the bridge effect of the crystals. In other words, the adjacent OMMT layers are linked by the PLA crystals that serve as a bridge with respect to the spaces between the OMMT layers. Therefore, when O_2 diffuses in such a structure, it should follow a considerably restrictive diffusional pathway, resulting in the reduced gas permeability of the composite film. If the orientation of the nanofiller is not perpendicular to the gas molecule diffusion direction, the Bharadwaj model can be considered to be a good fit to the experimental data.[41−43] This can be calculated using eqs 2 and 3[44]

$$\frac{P_S}{P_P} = \frac{1-\phi_S}{1+\frac{L}{2W}\phi_S\left(\frac{2}{3}\right)\left(S+\frac{1}{2}\right)} \tag{2}$$

$$S = \frac{1}{2}(3\cos^2\theta - 1) \tag{3}$$

where P_s and P_p are the permeabilities of the composite film and neat PLA, respectively, ϕ_S denotes the volume fraction of OMMT, and L/W denotes the aspect ratio (α), which can be defined as the ratio of the length to thickness of the impermeable flakes. S is the order parameter that is dependent on the orientation of nanoplatelets, where θ is the angle between the plane of the nanoplatelets and the perpendicular direction with respect to the diffusive gas molecules.

https://dx.doi.org/10.1021/acsomega.0c01405
ACS Omega 2020, 5, 18675−18684

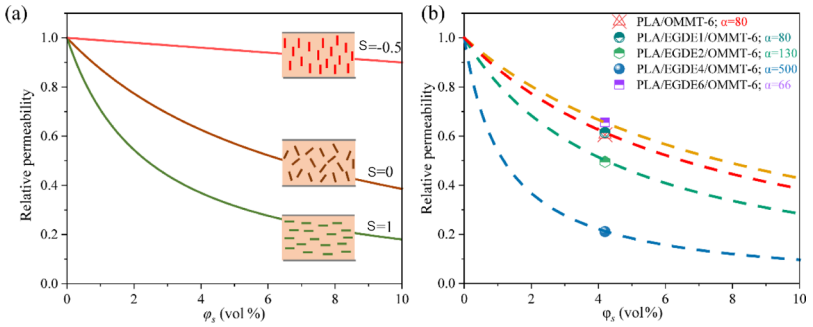

Figure 5. (a) Predictions of the Bharadwaj model for the relative permeability as a function of the volume fraction of the nanoplatelets for L/W = 80 and three different orientations and (b) comparison between the experimental data obtained with respect to P_{O_2} and the Bharadwaj model for the relative permeability in terms of the OMMT loadings.

We can calculate the volume fraction of the flakes in the polymer matrix using the following equation[45]

$$\phi_S = \frac{1}{1 + (\rho_S(1 - M_S)/\rho_P M_S)} \quad (4)$$

where ϕ_S is the volume fraction of OMMT, ρ_S and ρ_P denote the densities of OMMT and PLA, respectively, and M_S is the mass fraction of OMMT. The weight content of OMMT in the nanocomposites was converted to volume content using densities of 1.25 and 2.1 g/cm^3 for PLA and OMMT, respectively.[30,46]

Figure 5a shows the predicted dependency of the relative permeability (P_s/P_p) of PLA/OMMT on the OMMT loading (φ_s) when L/W is maintained constant at 80. The value of S is −0.5, and φ_s has little effect on the relative permeability when the orientation of the nanoplates is perpendicular to the film surface. The random orientation of the nanoplates resulted in an S value of 0; in this case, the relative permeability clearly decreased as a function of φ_s. When the orientation of the nanoplates was parallel to the film surface, S reached its maximum value of 1. A comparison between the experimental data obtained with respect to P_{O_2} and the Bharadwaj model for the relative permeability in terms of the OMMT loadings without EGDE is shown in Figure S2. When the OMMT content is 2, 4, and 6 wt %, our experimental data about the reduction in P_s/P_p are scattered randomly between the predicted Bharadwaj values in the case of S = 0 and S = 1, which suggest that OMMT is apt to randomly disperse throughout the PLA matrix. Figure S3 shows the transmission electron microscopy (TEM) image of PLA/OMMT-6, which shows the random dispersion of OMMT in the PLA matrix. However, when the OMMT content is 8 and 10 wt %, because of the aggregate effect, the Bharadwaj model is no longer applicable. Figure 5b shows the plot of the relative permeabilities P_s/P_p calculated based on the oxygen permeability as a function of φ_s using the Bharadwaj model with an S value of 0. For PLA/OMMT-6 and PLA/EGDE1/OMMT-6, the data were close to the Bharadwaj curve at α = 80. With an increase in the EGDE content, the data approached the curve at α = 130 and 500. However, the data approached the curve at α = 66 at an EGDE concentration of 6 phr.

Because the L/W value of a single OMMT layer is fixed, the increase in the α value can be attributed to the PLA crystals, which filled the spaces between two adjacent OMMT layers and served as a bridge to link the layers. Chen et al.[47] previously reported that when using isothermal recrystallization techniques, GO nanosheets could be linked using the poly(vinyl alcohol) (PVA) crystals that serve as a bridge at the spaces between the GO nanosheets. In view of this, the authors prepared a hybrid PVA/GO composite film exhibiting improved gas barrier properties. Here, the distance between two adjacent layers considerably influences the gas barrier performance of the nanocomposite films. Thus, if the distance between two adjacent layers is sufficiently close, they will be tightly connected by the PLA crystals. As depicted in Figure 5b, PLA/EGDE4/OMMT-6 showed the highest aspect ratio, which is in accordance with the XRD analysis, where this sample exhibited the lowest interlayer spacing. The closer the distance between the lamellae, the easier it can be filled by the crystals. Figure 6 shows the manner in which the adjacent

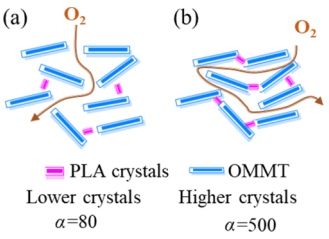

Figure 6. Illustration of the gas barrier film of the PLA/EGDE/OMMT nanocomposites with (a) low crystals and high interlayer spacing and (b) high crystals and low interlayer spacing linked by PLA crystals.

layers are connected by the PLA crystals and that the considerably low O_2 relative permeability can be attributed to the considerably long diffusion path in the PLA/EGDE4/OMMT-6 film.

3.4. Thermal and Mechanical Properties. We conducted thermogravimetric analysis (TGA) to study the thermal stability of PLA/OMMT and its nanocomposites with varying amounts of EGDE. The typical TGA data are presented in Table 5, whereas the TGA curves are shown in Figures 7 and S4. The initial thermal decomposition temperature (T_i) of PLA/OMMT-6 was 343.9 °C, at which a weight loss of 5% could be observed. With respect to the EGDE-containing nanocomposites, T_i gradually decreased with increasing EGDE. When adding 4 phr EGDE, T_i decreased from 343.9 to 338.5 °C. The thermal stability of the PLA/EGDE/OMMT nanocomposites deteriorated more than that of the nanocomposites without EGDE. The thermal stability deterioration can be attributed to the degradation of the EGDE hydroxyl groups obtained after epoxy ring opening. In addition, these

https://dx.doi.org/10.1021/acsomega.0c01405
ACS Omega 2020, 5, 18675−18684

Table 5. TGA Data for all the PLA/OMMT Composite Samples

samples	T_i (°C)	T_{max} (°C)
PLA	340	377
PLA/OMMT-2	341	380
PLA/OMMT-4	344	382
PLA/OMMT-6	345	383
PLA/OMMT-8	341	380
PLA/OMMT-10	339	381
PLA/EGDE1/OMMT-6	340	375
PLA/EGDE2/OMMT-6	340	375
PLA/EGDE4/OMMT-6	338	375
PLA/EGDE6/OMMT-6	331	375

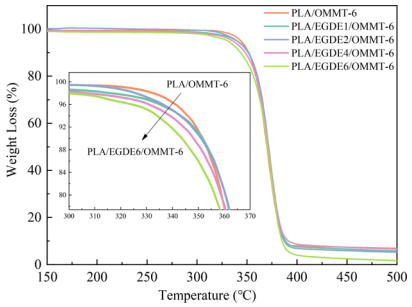

Figure 7. Thermal gravimetric curves of the PLA/OMMT-6 nanocomposites with different amounts of EGDE (10 °C/min under N_2).

hydroxyl groups can facilitate the degradation of the PLA matrix.[48] These two reasons caused the decrease in the thermal stability of nanocomposites after addition of EGDE. However, the reduction of the thermal decomposition temperature does not affect the use of the packaging film because its practical application temperature is considerably lower than the thermal decomposition temperature.

The tensile strength and elongation at break of the nanocomposites are shown in Figure 8. The tensile strength of PLA/OMMT-6 increased by 6.8 MPa when compared with that of neat PLA. However, the tensile strength of the composite was lower than that of neat PLA when the OMMT content was increased up to 10 wt %. Here, this is mainly because the increased aggregation in OMMT increased the concentration of defects, which decreased the tensile strength. However, after the addition of EGDE, the tensile strength decreased to become approximately 46 MPa. This deterioration in tensile strength can be mainly attributed to the degradation of PLA in the presence of hydroxyl groups when preparing nanocomposite films, which formed by epoxy ring opening of EGDE. Although the PLA/EGDE/OMMT films show a relatively lower tensile strength when compared with that shown by the neat PLA film, it is still in agreement with the actual requirements and is higher than that of the PE package film (22.5 MPa).[49] In addition, the elongation at break of PLA/OMMT-6 increased from 2.8 to 4.5% when compared with that observed in the case of neat PLA, and PLA/EGDE4/OMMT-6 showed approximately the same value as that shown by PLA/OMMT-6.

The SEM morphologies of the fracture surface with respect to neat PLA, PLA/OMMT-6, and PLA/EGDE4/OMMT-6 are presented in Figure 9. As shown in the SEM image of PLA/OMMT-6 (Figure 9b), a rough fractured surface can be observed, and OMMT displayed some aggregation in certain regions, which is in contrast with the smooth fractured surface of neat PLA. In terms of PLA/EGDE4/OMMT-6 (Figure 9c), a smooth fractured surface can be observed, and OMMT was largely individually exfoliated and dispersed in the PLA matrix with no suggestion of aggregation, which is in contrast with the smooth fractured surface of neat PLA.

4. CONCLUSIONS

In this work, the effect of the usage of OMMT nanoplates accompanied by the enhancement of the crystallinity on the barrier properties of PLA was investigated. EGDE was used to regulate the interlayer spacing of OMMT and increase the crystallinity of PLA to improve the gas barrier performance of the PLA/OMMT films. The crystallinity of PLA significantly improved because EGDE-modified OMMT served as an efficient nucleating agent for enhancing the crystallization. The PLA/EGDE/OMMT films had a unique structure, in which the adjacent OMMT layers were linked by the PLA crystals that served as a bridge at the spaces between the OMMT layers. The PLA/EGDE4/OMMT-6 film demonstrated an O_2 permeability reduction of approximately 79% when compared with the neat PLA film. The XRD and DSC analyses indicated that the reduced oxygen permeability of PLA/EGDE4/OMMT-6 was primarily a consequence of the high crystallinity of the PLA matrix and the bridging effect of the PLA crystals between two adjacent layers. Based on the experimental results, the relation between relative permeability and vol % OMMT was in good agreement with those of the predicted values using the Bharadwaj model when $S = 0$. The added EGDE deteriorated the thermal stability, mainly because of the degradation of the hydroxyl groups of EGDE formed by

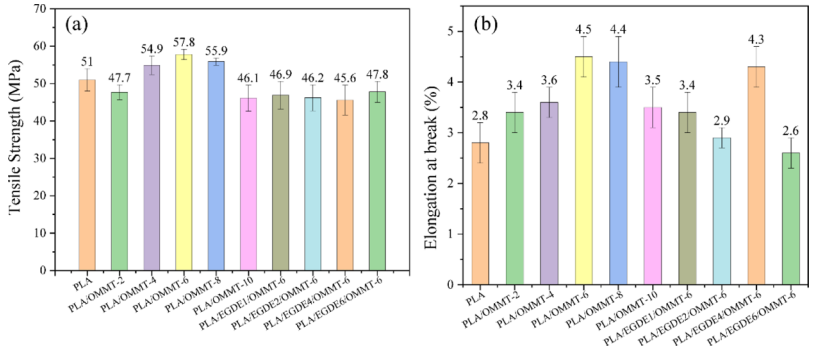

Figure 8. (a) Tensile strength and (b) elongation at break of the nanocomposites.

https://dx.doi.org/10.1021/acsomega.0c01405
ACS Omega 2020, 5, 18675−18684

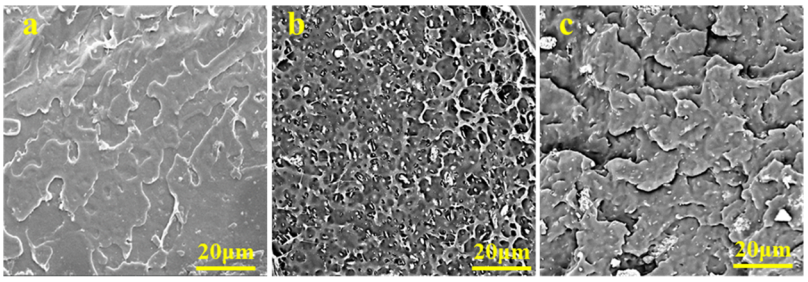

Figure 9. Typical SEM images for the fractured surfaces of (a) neat PLA, (b) PLA/OMMT-6, and (c) PLA/EGDE4/OMMT-6.

epoxy ring opening, whereas these hydroxyl groups can further promote the degradation of the PLA matrix. However, the practical application temperature of the packaging film is considerably lower than the thermal decomposition temperature; therefore, the reduction of the thermal decomposition temperature does not affect the usage of packaging films.

■ ASSOCIATED CONTENT

Supporting Information

The Supporting Information is available free of charge at https://pubs.acs.org/doi/10.1021/acsomega.0c01405.

ATR spectra, comparison between the experimental data obtained with respect to P_{O_2} and the Bharadwaj model for the relative permeability in terms of the OMMT loadings, TEM images of PLA/OMMT-6, and TGA curves of PLA and PLA/OMMT nanocomposites with different amounts of OMMT (PDF)

■ AUTHOR INFORMATION

Corresponding Authors

Caili Zhang − *College of Chemistry and Materials Engineering and Beijing Key Laboratory of Quality Evaluation Technology for Hygiene and Safety of Plastics, Beijing Technology and Business University, Beijing 100048, China;* orcid.org/0000-0003-0938-2415; Email: zhangcaili@btbu.edu.cn

Yunxuan Weng − *College of Chemistry and Materials Engineering and Beijing Key Laboratory of Quality Evaluation Technology for Hygiene and Safety of Plastics, Beijing Technology and Business University, Beijing 100048, China;* Email: wyxuan@th.btbu.edu.cn

Author

Fenfen Li − *College of Chemistry and Materials Engineering, Beijing Technology and Business University, Beijing 100048, China*

Complete contact information is available at: https://pubs.acs.org/10.1021/acsomega.0c01405

Notes

The authors declare no competing financial interest.

■ ACKNOWLEDGMENTS

We are grateful to the financial support from the National Natural Science Foundation of China (grant numbers: 51773005, 21905008), the Beijing Natural Science Foundation (grant number: 2194071), and the National Key Research and Development Program of China (grant number: 2019YFD1101201).

■ REFERENCES

(1) Silvestre, C.; Duraccio, D.; Cimmino, S. Food packaging based on polymer nanomaterials. *Prog. Polym. Sci.* **2011**, *36*, 1766−1782.
(2) Youssef, A. M.; El-Sayed, S. M. Bionanocomposites materials for food packaging applications: Concepts and future outlook. *Carbohydr. Polym.* **2018**, *193*, 19−27.
(3) Lambert, S.; Wagner, M. Environmental performance of bio-based and biodegradable plastics: the road ahead. *Chem. Soc. Rev.* **2017**, *46*, 6855−6871.
(4) He, X.; Hwang, H.-M. Nanotechnology in food science: Functionality, applicability, and safety assessment. *J. Food Drug Anal.* **2016**, *24*, 671−681.
(5) Weng, Y.-X.; Jin, Y.-J.; Meng, Q.-Y.; Wang, L.; Zhang, M.; Wang, Y.-Z. Biodegradation behavior of poly (butylene adipate-co-terephthalate)(PBAT), poly (lactic acid)(PLA), and their blend under soil conditions. *Polym. Test.* **2013**, *32*, 918−926.
(6) Drumright, R. E.; Gruber, P. R.; Henton, D. E. Polylactic acid technology. *Adv. Mater.* **2000**, *12*, 1841−1846.
(7) Garlotta, D. A literature review of poly (lactic acid). *J. Polym. Environ.* **2001**, *9*, 63−84.
(8) Tang, X. Z.; Kumar, P.; Alavi, S.; Sandeep, K. P. Recent advances in biopolymers and biopolymer-based nanocomposites for food packaging materials. *Crit. Rev. Food Sci. Nutr.* **2012**, *52*, 426−442.
(9) Zeng, Q. H.; Yu, A. B.; Lu, G. Q.; Paul, D. R. Clay-based polymer nanocomposites: research and commercial development. *J. Nanosci. Nanotechnol.* **2005**, *5*, 1574−1592.
(10) Cui, Y.; Kumar, S.; Rao Kona, B.; van Houcke, D. Gas barrier properties of polymer/clay nanocomposites. *RSC Adv.* **2015**, *5*, 63669−63690.
(11) Tan, B.; Thomas, N. L. A review of the water barrier properties of polymer/clay and polymer/graphene nanocomposites. *J. Membr. Sci.* **2016**, *514*, 595−612.
(12) De Paiva, L. B.; Morales, A. R.; Valenzuela Díaz, F. R. Organoclays: properties, preparation and applications. *Appl. Clay Sci.* **2008**, *42*, 8−24.
(13) Vaia, R. A.; Giannelis, E. P. Polymer melt intercalation in organically-modified layered silicates: model predictions and experiment. *Macromolecules* **1997**, *30*, 8000−8009.
(14) Herrera-Alonso, J. M.; Marand, E.; Little, J. C.; Cox, S. S. Transport properties in polyurethane/clay nanocomposites as barrier materials: effect of processing conditions. *J. Membr. Sci.* **2009**, *337*, 208−214.
(15) Sanchez-Garcia, M. D.; Gimenez, E.; Lagaron, J. Morphology and barrier properties of nanobiocomposites of poly (3-hydroxybutyrate) and layered silicates. *J. Appl. Polym. Sci.* **2008**, *108*, 2787−2801.
(16) Rhim, J.-W.; Hong, S.-I.; Ha, C.-S. Tensile, water vapor barrier and antimicrobial properties of PLA/nanoclay composite films. *LWT−Food Sci. Technol.* **2009**, *42*, 612−617.
(17) Koh, H. C.; Park, J. S.; Jeong, M. A.; Hwang, H. Y.; Hong, Y. T.; Ha, S. Y.; Nam, S. Y. Preparation and gas permeation properties of biodegradable polymer/layered silicate nanocomposite membranes. *Desalination* **2008**, *233*, 201−209.
(18) Sabet, S. S.; Katbab, A. A. Interfacially compatibilized poly (lactic acid) and poly (lactic acid)/polycaprolactone/organoclay

https://dx.doi.org/10.1021/acsomega.0c01405
ACS Omega 2020, 5, 18675−18684

nanocomposites with improved biodegradability and barrier properties: effects of the compatibilizer structural parameters and feeding route. *J. Appl. Polym. Sci.* **2009**, *111*, 1954−1963.
(19) Ray, S. S.; Yamada, K.; Okamoto, M.; Ueda, K. New polylactide-layered silicate nanocomposites. 2. Concurrent improvements of material properties, biodegradability and melt rheology. *Polymer* **2003**, *44*, 857−866.
(20) Picard, E.; Espuche, E.; Fulchiron, R. Effect of an organo-modified montmorillonite on PLA crystallization and gas barrier properties. *Appl. Clay Sci.* **2011**, *53*, 58−65.
(21) Wolf, C.; Angellier-Coussy, H.; Gontard, N.; Doghieri, F.; Guillard, V. How the shape of fillers affects the barrier properties of polymer/non-porous particles nanocomposites: A review. *J. Membr. Sci.* **2018**, *556*, 393−418.
(22) Li, J.; Lai, L.; Wu, L.; Severtson, S. J.; Wang, W.-J. Enhancement of water vapor barrier properties of biodegradable poly (butylene adipate-co-terephthalate) films with highly oriented organomontmorillonite. *ACS Sustainable Chem. Eng.* **2018**, *6*, 6654−6662.
(23) Choudalakis, G.; Gotsis, A. D. Permeability of polymer/clay nanocomposites: a review. *Eur. Polym. J.* **2009**, *45*, 967−984.
(24) Fortunati, E.; Armentano, I.; Zhou, Q.; Puglia, D.; Terenzi, A.; Berglund, L. A.; Kenny, J. M. Microstructure and nonisothermal cold crystallization of PLA composites based on silver nanoparticles and nanocrystalline cellulose. *Polym. Degrad. Stab.* **2012**, *97*, 2027−2036.
(25) Abdellatief, A.; Welt, B. A. Comparison of new dynamic accumulation method for measuring oxygen transmission rate of packaging against the steady-state method described by ASTM D3985. *Packag. Technol. Sci.* **2013**, *26*, 281−288.
(26) Lotz, B.; Li, G.; Chen, X.; Puiggali, J. Crystal polymorphism of polylactides and poly (Pro-alt-CO): The metastable beta and gamma phases. Formation of homochiral PLLA phases in the PLLA/PDLA blends. *Polymer* **2017**, *115*, 204−210.
(27) Kovalcik, A.; Pérez-Camargo, R. A.; Fürst, C.; Kucharczyk, P.; Müller, A. J. Nucleating efficiency and thermal stability of industrial non-purified lignins and ultrafine talc in poly (lactic acid)(PLA). *Polym. Degrad. Stab.* **2017**, *142*, 244−254.
(28) Tsuji, H.; Okino, R.; Daimon, H.; Fujie, K. Water vapor permeability of poly (lactide) s: Effects of molecular characteristics and crystallinity. *J. Appl. Polym. Sci.* **2006**, *99*, 2245−2252.
(29) Ding, C.; Jia, D.; He, H.; Guo, B.; Hong, H. How organo-montmorillonite truly affects the structure and properties of polypropylene. *Polym. Test.* **2005**, *24*, 94−100.
(30) Huang, H.-D.; Ren, P.-G.; Xu, J.-Z.; Xu, L.; Zhong, G.-J.; Hsiao, B. S.; Li, Z.-M. Improved barrier properties of poly (lactic acid) with randomly dispersed graphene oxide nanosheets. *J. Membr. Sci.* **2014**, *464*, 110−118.
(31) Pinto, A. M.; Cabral, J.; Tanaka, D. A. P.; Mendes, A. M.; Magalhães, F. D. Effect of incorporation of graphene oxide and graphene nanoplatelets on mechanical and gas permeability properties of poly (lactic acid) films. *Polym. Int.* **2013**, *62*, 33−40.
(32) Meares, P. The diffusion of gases through polyvinyl acetate1. *J. Am. Chem. Soc.* **1954**, *76*, 3415−3422.
(33) Haraya, K.; Hwang, S.-T. Permeation of oxygen, argon and nitrogen through polymer membranes. *J. Membr. Sci.* **1992**, *71*, 13−27.
(34) Weller, S.; Steiner, W. A. Separation of gases by fractional permeation through membranes. *J. Appl. Phys.* **1950**, *21*, 279−283.
(35) Haraya, K.; Obata, K.; Hakuta, T.; Yoshitome, H. Permeation of gases through a symmetric cellulose acetate membrane. *J. Chem. Eng. Jpn.* **1986**, *19*, 464−466.
(36) Michaels, A. S.; Vieth, W. R.; Barrie, J. A. Solution of gases in polyethylene terephthalate. *J. Appl. Phys.* **1963**, *34*, 1−12.
(37) Tikhomirov, B. P.; Hopfenberg, H. B.; Stannett, V.; Williams, J. L. Permeation, diffusion, and solution of gases and water vapor in unplasticized poly (vinylchloride). *Die Makromol. Chem.* **1968**, *118*, 177−188.
(38) Hwang, S. T.; Choi, C. K.; Kammermeyer, K. Gaseous transfer coefficients in membranes. *Anal. Lett., Part A* **1974**, *9*, 461−478.
(39) El-Hibri, M. J.; Paul, D. R. Gas transport in poly (vinylidene fluoride): effects of uniaxial drawing and processing temperature. *J. Appl. Polym. Sci.* **1986**, *31*, 2533−2560.
(40) Cui, Y.; Kundalwal, S. I.; Kumar, S. Gas barrier performance of graphene/polymer nanocomposites. *Carbon* **2016**, *98*, 313−333.
(41) Tenn, N.; Follain, N.; Soulestin, J.; Crétois, R.; Bourbigot, S.; Marais, S. Effect of nanoclay hydration on barrier properties of PLA/montmorillonite based nanocomposites. *J. Phys. Chem. C* **2013**, *117*, 12117−12135.
(42) Chien, A.-T.; Lin, K.-F. Morphology and permeability of exfoliated PVAc-MMT nanocomposite films cast from soap-free emulsion-polymerized latices. *J. Polym. Sci., Part A: Polym. Chem.* **2007**, *45*, 5583−5589.
(43) Alix, S.; Follain, N.; Tenn, N.; Alexandre, B.; Bourbigot, S.; Soulestin, J.; Marais, S. Effect of highly exfoliated and oriented organoclays on the barrier properties of polyamide 6 based nanocomposites. *J. Phys. Chem. C* **2012**, *116*, 4937−4947.
(44) Bharadwaj, R. K. Modeling the barrier properties of polymer-layered silicate nanocomposites. *Macromolecules* **2001**, *34*, 9189−9192.
(45) Chen, B.; Evans, J. R. G. Nominal and effective volume fractions in polymer−clay nanocomposites. *Macromolecules* **2006**, *39*, 1790−1796.
(46) Liu, G.; Song, Y.; Wang, J.; Zhuang, H.; Ma, L.; Li, C.; Liu, Y.; Zhang, J. Effects of nanoclay type on the physical and antimicrobial properties of PVOH-based nanocomposite films. *LWT–Food Sci. Technol.* **2014**, *57*, 562−568.
(47) Chen, J.-T.; Fu, Y.-J.; An, Q.-F.; Lo, S.-C.; Zhong, Y.-Z.; Hu, C.-C.; Lee, K.-R.; Lai, J.-Y. Enhancing polymer/graphene oxide gas barrier film properties by introducing new crystals. *Carbon* **2014**, *75*, 443−451.
(48) Bigg, D. M.; Sinclair, R. G.; Lipinsky, E. S.; Litchfield, J. H.; Allen, B. R., Degradation control of environmentally degradable disposable materials. U.S. Patent 6,323,307 B1.2001.
(49) Dintcheva, N. T.; La Mantia, F. P.; Malatesta, V. Photo-oxidation behaviour of polyethylene/multi-wall carbon nanotube composite films. *Polym. Degrad. Stab.* **2009**, *94*, 162−170.

https://dx.doi.org/10.1021/acsomega.0c01405
ACS Omega 2020, 5, 18675−18684